ACS APPLIED MATERIALS & INTERFACES

Research Article

www.acsami.org

Large-Amplitude, Reversible, pH-Triggered Wetting Transitions Enabled by Layer-by-Layer Films

Yiming Lu,[†] Mohammad Amin Sarshar,[‡] Ke Du,[‡] Tsengming Chou,[§] Chang-Hwan Choi,*[,‡] and Svetlana A. Sukhishvili[†,]*

[†]Department of Chemistry, Chemical Biology and Biomedical Engineering, [‡]Department of Mechanical Engineering, and [§]Department of Chemical Engineering and Material Science, Stevens Institute of Technology, Hoboken, New Jersey 07030, United States

Supporting Information

ABSTRACT: We report on the use of layer-by-layer (LbL) hydrogels, composed of amphiphilic polymers that undergo reversible collapse-dissolution transition in solutions as a function of pH, to induce sharp, large-amplitude wetting transition at microstructured surfaces. Surface hydrogels were composed of poly(2-alkylacrylic acids) (PaAAs) of varied hydrophobicity, i.e., poly(methacrylic acid) (PMAA), poly(2-ethylacrylic acid) (PEAA), poly(2-n-propylacrylic acid) (PPAA) and poly(2-n-butylacrylic acid) (PBAA). When deposited at a micropillar-patterned silicon substrate, hydrophilic PMAA LbL hydrogels supported complete surface wetting (contact angle, CA, of 0°), whereas PEAA, PPAA, and PBAA ultrathin coatings supported large-amplitude wetting transitions, with CA changes from 110 to 125° at acidic to 0° at basic pH values, and the transition pH increasing from 6.2 to 8.4 with increased polyacid hydrophobicity. At acidic pHs, droplets showed a large hysteresis in CA (a "sticky droplet" behavior), and remained in the Wenzel state. The fact that CA changes for wetting-nonwetting transitions occurred at values close to physiologic pH makes these coatings promising for controlling flow and bioadhesion using external stimuli. Finally, we show that the surface wettability transitions can be used to detect positively charged analytes (such as gentamicin) in solution via large changes in CA associated with adsorption of analytes within the hydrogels.

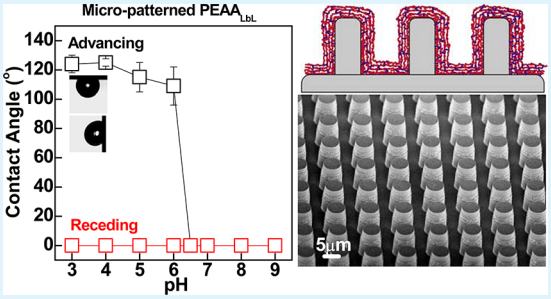

KEYWORDS: *layer-by-layer, stimuli-responsive, wettability, weak polyelectrolytes, surface hydrogels*

INTRODUCTION

Surface wettability is central to a wide range of events occurring in nature. Rice and lotus leaves, butterfly wings, bird feathers and insect bodies are just few examples that exploit surface properties to control water adhesion.[1] Man-made superhydrophobic surfaces that often mimic behavior of these natural interfaces, which support complete roll off of water droplets, have been widely studied, often with the goal of making superhydrophobic water-repelling[2−7] or omniphobic self-cleaning materials,[8] or controlling biological adhesion.[9] However, pinning of water droplets is also exploited in natural processes, for example in collection of water droplets by rose petals and cactus leaves.[10] Designing versatile surfaces that support "sticky" droplets, but go beyond that by manipulating the droplet wetting properties via external stimuli is a promising direction, which might enable new "intelligent" microfluidic devices and diagnostic chips. While self-cleaning superhydrophobic surfaces reside in a Cassie−Baxter state with a water contact angle (CA) over 150° and low contact angle hysteresis (CAH),[11] controlled deposition of water droplets for microfluidic and biochip applications relies on a different wetting state, the Wenzel state,[12] which exhibits a high CAH due to a strong contact line pinning.

Several approaches have been used to create tunable hydrophobic and superhydrophobic surfaces.[13] In the case of hydrophobic fabric, for example, changes in wettability can be achieved via simple mechanical stretching.[14] At smooth surfaces, irreversible changes in surface wettability have been used to detect specific binding of a biological ligand within a monolayer-immobilized receptor.[15] By using inorganic nanostructured substrates, such as ZnO micropillars,[16] or Si nanowires and nickel micronails coated with nonresponsive organic coatings, tunable wettability of surfaces can be achieved via application of light,[17] electrical voltage,[18] or magnetic field.[19] Responsive, ultrathin organic coatings, such as photoswitchable azobenzene coatings, have also been used to endow surfaces with response to UV irradiation.[20] With monolayers of dendric thiols with carboxyl functionality adsorbed at gold roughened substrates, wettability transition occurred only at very high pH values.[21]

The use of responsive polymers as building blocks of surface coatings presents a versatile approach to control surface wettability and mechanical properties, and is specifically suited

Received: September 11, 2013
Accepted: November 5, 2013
Published: November 5, 2013

for the application of biologically relevant pH or temperature stimuli. The most well-known type of such "intelligent" coatings is surface-grafted environmentally responsive polymer brushes. If grafted polymer chains undergo hydrophilic-to-hydrophobic transition as a result of external stimuli, significant changes in surface wettability result.[22] For example, the lower critical solution temperature (LCST) behavior of poly(N-isopropylacrylamide) (PNIPAM), and pH-triggered collapse of a positively charged polyelectrolyte were used for switching surface wetting properties.[23,24] Polymer brush with dual temperature and pH response was also used to induce surface hydrophobicity−hydrophilicity transitions.[25] Although promising, grafting polymer brushes of diverse functionality, which supports environmentally triggered collapse of polymer chains in an aqueous environment, usually involves complicated synthetic procedures, often not readily transferable to modification of large-surface-area planar or microporous substrates, as well as microchannels.

An alternative, chemically more versatile, approach to modifying surface properties of large-area substrates of arbitrary shape, porosity and chemistry is the layer-by-layer (LbL) assembly of polyelectrolytes.[26,27] This nonline-of-sight technique enables inclusion of a broad range of synthetic, biological polymers and/or nanoparticles within functional surface coatings. Several reports have demonstrated construction of superhydrophobic surfaces based on LbL-coated films. One often used strategy includes "roughening" polyelectrolyte multilayers (PEMs) via inorganic nanostructures, introduction of porosity within PEM films, and/or film deposition on nanofibrous substrate, followed by surface hydrophobization.[28−32] Alternatively, a hydrophobic fluorinated polymer, Nafion, can be directly included within roughened LbL films.[33]

Although PEMs present a powerful and versatile platform for constructing superhydrophobic surfaces, controlling surface wettability of PEM coatings via external stimuli has remained a challenge. The main limitation is that intermolecular binding between polymers, a feature that assures stability of LbL films, becomes a major roadblock for constructing coatings capable of switching the surface wetting behavior. Indeed, it has been shown that CAs of poly(acrylic acid) (PAA)/polyallylamine hydrochloride (PAH) multilayer films are strongly dependent on the multilayer deposition conditions, such as pH and salt concentration, and also vary with the type of the outermost polyelectrolyte layer within PEM films.[34] With deposited PEM films, however, film response is usually hampered by intermolecular polyelectrolyte binding. Mechanical stretching was applied to Nafion-containing LbL film to achieve tunable surface wettability as a result of surface reconstruction.[35] With nonstretchable PEM-coated substrates, some success has been achieved with "roughened" PEMs of a cationic copolymer of NIPAM and Nafion, which showed ∼40° changes in the CA upon variation of temperature.[36] To achieve larger-amplitude wettability transitions with PEMs, it was necessary to employ ion exchange involving hydrophobic fluoro-containing counterions.[37,38]

Here, we report a general approach to control wettability of surfaces via pH-induced collapse/solubilization of polymer units within single-component surface-bound LbL hydrogels. Unlike the counterion exchange approach based on the use of a very specific type of toxic fluoro-containing ions, pH variations are versatile and environmentally benign. The fact that changes in acidity are ubiquitous in nature makes us believe that wettability transition reported here can be triggered not only by external pH variations, but also by "internal" pH changes associated with specific biological events such as biofilm growth, or other biological or environmental events. Our approach is based on constructing chemically cross-linked ultrathin LbL hydrogels, composed of amphiphilic polymers which undergo reversible collapse-dissolution transition in solutions as a function of external stimuli (in our case, pH). Note that conformal coating of microstructured substrates with ultrathin hydrogels of controlled thickness cannot be achieved using conventional bulk hydrogels. Our hydrogels were fabricated based on hydrogen-bonded LbL films[39] via selective chemical cross-linking of a polycarboxylic acid component, followed by release of neutral hydrogen-bonded chains. While non-LbL, as well as LbL surface hydrogels have been reported earlier by several groups,[40] including ours,[41] here we exclusively focus on the type of macromolecules which reversibly collapse/hydrate in aqueous solutions in response to external stimuli. Such polymers include several homopolymers of 2-alkylacrylic acids with a general abbreviation PaAA, such as poly(2-ethylacrylic acid) (PEAA), poly(2-*n*-propylacrylic acid) (PPAA), and poly(2-*n*-butylacrylic acid) (PBAA). Unlike their better known, more hydrophilic PaAA counterparts (PAA and poly(methacrylic acid) (PMAA)), these amphiphilic polycarboxylic acids become hydrophobic and precipitate from solutions at slightly acidic pHs. Most recently, we have reported on PEAA homopolymer brushes, which remained relatively hydrophobic in the entire range of pH, exhibiting only ∼8° changes in CA upon pH variations.[42] Here we show that the use of PaAAs for constructing LbL hydrogel coatings ($PEAA_{LbL}$, $PPAA_{LbL}$, and $PBAA_{LbL}$) on micropatterned substrates results in highly functional coatings, which support large-amplitude (CAs change from ∼120° to 0°) surface wettability transitions. The occurrence of the transition on the pH scale can be controlled via hydrophobicity of PaAA coatings. Moreover, the fact that CA changes for wetting−nonwetting transition of $PEAA_{LbL}$ and $PPAA_{LbL}$ hydrogel films occurred at values close to physiologic pH (between 5.5 and 7.5), makes these coatings promising for controlling flow and bioadhesion using external stimuli.

EXPERIMENTAL SECTION

Materials. PMAA (M_w ≈ 56 000 g/mol), branched poly(ethylene imine) (BPEI) (M_w ≈ 101 000 g/mol), polyvinylpyrrolidone (PVPON) (M_w ≈ 2500 g/mol), monobasic sodium phosphate, 1-ethyl-3-(3-dimethylaminopropyl)carbodiimide hydrochloride (EDC), adipic acid dihydrazide (AADH), hydrochloric acid, sodium hydroxide, gentamicin (10 mg/mL in water), methanol, N,N-dimethylformamide (DMF) and dimethyl sulfoxide (DMSO) were purchased from Sigma. PEAA (M_w ≈ 79 000 g/mol), PPAA (M_w ≈ 110 000 g/mol), and PBAA (M_w ≈ 138 000) were synthesized following the procedure reported elsewhere.[43] The molecular weights of PaAAs were determined by GPC at a flow rate of 1 mL/min and 60 °C using 0.01 mM LiBr, DMF as a solvent, and polystyrene standards for column calibration. Millipore (Milli-Q system) filtered water with a resistivity of 18.2 MΩ was used in all experiments. Undoped silicon substrates of 525 ± 25 μm thickness were purchased from Virginia Semiconductor Inc.

Preparation of Micropatterned Silicon Substrates. The silicon microarray patterns were created by using standard photolithography and deep reactive ion etching (DRIE). A new silicon wafer was cleaned by using acetone and deionized water, followed by N_2 drying. SPR 3012 positive photoresist (Shipley Megaposit) was spun on the silicon wafer at 2000 rpm for 60 s, and the substrate was baked on a hot plate at 95 °C for 1 min. The photoresist layer was exposed to UV light using a mask aligner (Karl Suss MA6) with a soft contact mode with a gap of 40 μm. After postexposure bake on a hot plate at 115 °C for 1

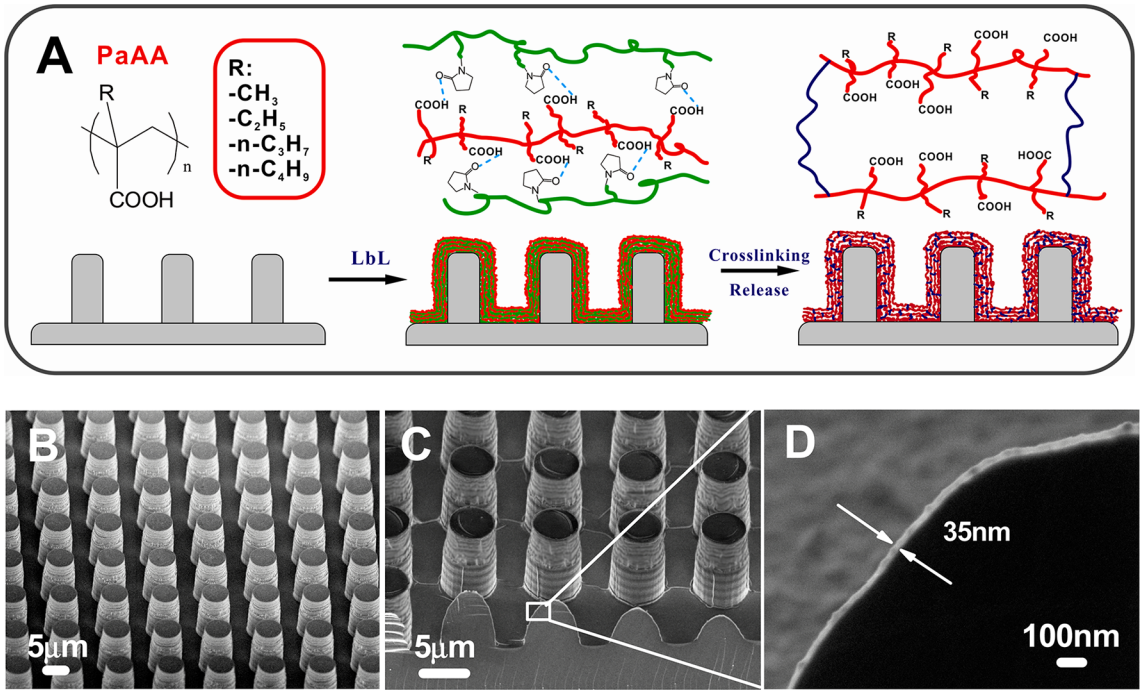

Figure 1. (A) Chemical structure, composition, and schematic representation of construction of single-component surface hydrogels on a micropillar-patterned substrate (PaAA is shown in red, PVPON in green, and a cross-linker in blue), (B) SEM image of a micropillar-patterned Si substrate with no coating, (C, D) SEM images of the micropatterned Si substrate after $PEAA_{LbL}$ coating.

min, the photoresist layer was developed in MF-319 developer solution (Shipley Megaposit) for 1−2 min. Finally, it was hard-baked on a hot plate at 110 °C for 1 min. The silicon substrate was then etched by using the patterned photoresist layer as etch mask in a DRIE process (PlasmaLab, Oxford Instruments). For the DRIE, a cryogenic etching process was employed at −100 °C, using SF_6 and O_2 gases. The etching depth is ∼15 μm for all the samples used in this paper.

Construction of Surface Hydrogels. Both micropatterned and nonpatterned silicon substrates were pretreated in ozone plasma and piranha solution (1:3 v/v H_2O_2:H_2SO_4) at least 3 times before use. Prior to multilayer construction, a bilayer of $(PMAA/BPEI)_2$ was deposited and cross-linked as reported elsewhere.[41] PaAA/PVPON multilayers were deposited from 0.5 mg/mL solutions in methanol, except for PMAA/PVPON films which were deposited from 0.01 M phosphate buffer solutions at pH 2. After EDC (3 mg/mL) activation at pH 5.2, both multilayers were cross-linked in AADH (3 mg/mL) for 3 h. To release PVPON, substrates were immersed in pH 7.5 buffer (for $PMAA_{LbL}$), or a mixture of pH 6 phosphate buffer (0.005M) and DMSO (1:5 v/v) (for $PaAA_{LbL}$) for 30 min, washed with water, methanol, and dried.

Surface and Film Characterization. Film thickness was measured by phase-modulated ellipsometry with an incident angle at 65°, assuming a constant film refractive index of 1.500. FTIR spectra were acquired using Tensor 27 FTIR spectrometer (Bruker Optik GmbH) operating in a transmission mode. Apparent CAs were measured in a room condition (temperature, ∼22 °C; humidity, 23% RH) using a goniometer (Rame-Hart 100−25-A). Advancing and receding CAs were measured by volume expansion/reduction method. All samples were pretreated by 0.01 M phosphate buffer solution with the same pH as used in the CA measurements. The CAs were measured 3 times at different positions of the samples and the average values were used for data interpretation. The SEM images of the silicon microstructures (coated and uncoated) were taken using an Auriga Cross-beam Microscope (Carl Zeiss Microscopy, GmbH). The imaging voltage was set at 2 kV and a secondary electron detector was used. All the samples were mounted on a 45° pretilted holder to obtain cross-section viewed images. Cryo-SEM was also carried out using the Auriga microscope equipped with a Leica cryo-transfer system (VCT-100 and MED-020, Leica Microsystems, GmbH) at 5 KV imaging voltage. Samples with a drop of buffer were plunge frozen in liquid nitrogen, transferred, and then imaged in SEM at −135 °C. AFM was used to characterize morphology of wet PaAA hydrogels at high pH using an NSCRIPTOR dip pen nanolithography system (Nanoink). The in situ AFM measurements were performed in the contact mode using P-MAN-SICT-0 AFM cantilevers (Pacific Nanotechnology, Inc.) with a force constant of 0.2 N/m.

RESULTS AND DISCUSSION

Figure 1A illustrates the construction of hydrogen-bonded multilayers on a micropillar-patterned silicon (Si) substrate. The micropillar pattern of a square array has been fabricated using photolithographic process and deep reactive ion etching. The diameter of pillar structure and the gap between pillars were 5 μm, and the height of the pillars was ∼15 μm (Figure 1B). For ellipsometric characterization of the deposited film thickness and swelling, we have also used planar, non-microstructured silicon wafers. After deposition of a ∼3.4 nm thick BPEI/PMAA precursor layer and its thermal cross-linking,[41] PaAA hydrogels were constructed based on PaAA/PVPON hydrogen-bonded films using chemical cross-linking as described in the Experimental Section. An example of monitoring the coating synthesis is shown in Figure S1 for PEAA/PVPON system. FTIR data in Figure S1 in the Supporting Information suggest complete release of PVPON from the cross-linked hydrogen-bonded films. For all $(PaAA/PVPON)_{15}$ films, the dry film thickness decreased from 55 ± 4 nm to 35 ± 4 nm (see Figure S2 in the Supporting Information), further confirming conversion of hydrogen-bonded PaAA/PVPON multilayers to $PaAA_{LbL}$ hydrogel films. The scanning electron microscopy (SEM) image also shows the same coating thickness on the micropillar-patterned substrate (Figure 1C-D). For control experiments, we have also prepared hydrophilic $PMAA_{LbL}$ hydrogels with matched dry thickness of ∼35 nm using the reported procedure.[41] Because

dx.doi.org/10.1021/am403944m | ACS Appl. Mater. Interfaces 2013, 5, 12617−12623

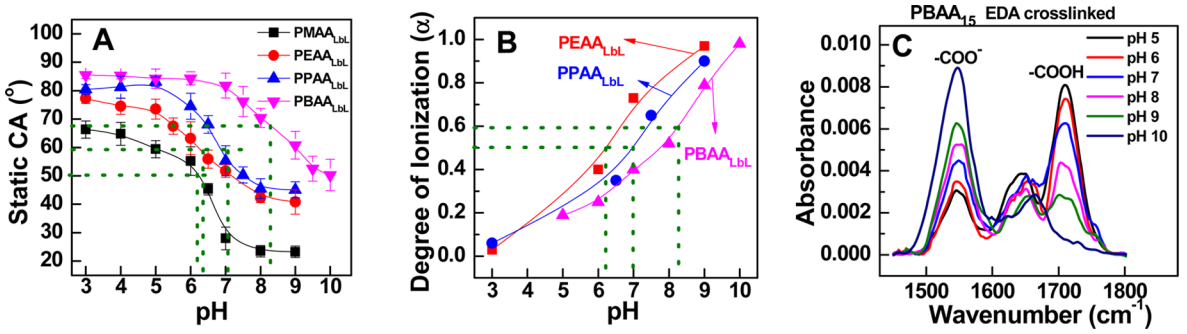

Figure 2. (A) Static CAs of PaAA$_{LbL}$-coated unpatterned substrates as a function of pH. The dotted lines indicate the contact angles at pH$_{tr}$. (B) The degree of ionization of PaAA$_{LbL}$ hydrogels deposited on unpatterned substrates as a function of pH. Ionization degree was calculated using the ratio of extinction coefficients between carboxylic (−COOH) and carboxylate (−COO$^-$) groups of 0.92. The dotted lines indicate ionization degrees corresponding to pH$_{tr}$. (C) FTIR spectra of a PBAA$_{LbL}$ film pre-exposed to solutions at various pH values prior to drying.

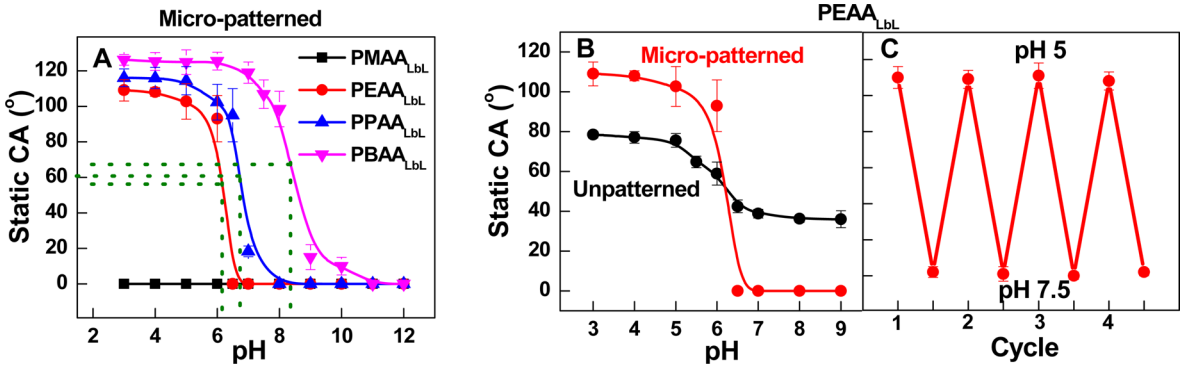

Figure 3. (A) Static CAs of PaAA$_{LbL}$-coated micropillared substrates with a square array of cylindrical pillar structures of ∼15 μm tall, 5 μm in diameter, and 5 μm in interpillar spcaing. (B) Static CAs of PEAA$_{LbL}$-coated micropillar-patterned and unpatterned substrates. (C) Reversible changes in CA of PEAA$_{LbL}$-coated micropillar-patterned substrate occurring between pH 5 and pH 7.5. All coatings had matched dry thickness of 35 ± 4 nm.

bilayer thickness in PMAA/PVPON films was higher (∼5.5 nm versus ∼3.7 nm for the PaAA/PVPON systems), only 10 bilayers were required for constructing matched-thickness PMAA$_{LbL}$ hydrogels.

We first explored wettability and ionization properties of PaAA$_{LbL}$ hydrogels deposited on smooth substrates. All PaAA$_{LbL}$ hydrogels exhibited a significant, 30−40°, change in CA as a result of pH-induced protonation/deprotonation of functional groups within PaAA$_{LbL}$ films (Figure 2A). The pH of the wettability transition, pH$_{tr}$, defined as the pH at the transition half-height was dependent on polyacid hydrophobicity, and increased from 6.3 to 7.1 and 8.3, for PEAA$_{LbL}$, PPAA$_{LbL}$, and PBAA$_{LbL}$ coatings, respectively. Although the pH$_{tr}$ (∼6.2) of PMAA$_{LbL}$ was very close to that of PEAA$_{LbL}$, PMAA$_{LbL}$ was more hydrophilic than the other PaAA$_{LbL}$ hydrogels in the whole pH range. Such a difference in surface wettability correlates with the solution behavior of PaAA coatings. As determined for 3 mg/mL PaAA solutions, while PMAA remains soluble in water at any pH values, more hydrophobic polyacids precipitate from solutions with pH <5.2−5.8,[44] <5.5−5.9, and <6.5−7.0 for PEAA, PPAA, and PBAA, respectively. As shown in Figure 2B, pH$_{tr}$ corresponded to pK$_a$ of LbL hydrogels (ionization degree of 50%) in the case of PEAA$_{LbL}$ and PPAA$_{LbL}$ films, but a higher ionization of ∼60% had to be achieved to switch to a relatively hydrophilic state with more hydrophobic PBAA$_{LbL}$ hydrogels.

After deposition on the micropillared substrate (Figure 3), coatings constructed from hydrophobic polyacids (PEAA$_{LbL}$, PPAA$_{LbL}$, or PBAA$_{LbL}$) all showed large-amplitude pH-triggered wetting transitions, while a more hydrophilic PMAA$_{LbL}$ film supported complete surface wetting (CA of 0°) within the entire range of pH (Figure 3A). This phenomenon is because PMAA chains remain highly hydrated and do not precipitate at acidic pH values. Wettability transition pH values pH$_{tr}$ of 6.2, 7.0, and 8.4, observed for PEAA$_{LbL}$, PPAA$_{LbL}$, and PBAA$_{LbL}$, respectively, were very close to those found with unpatterned surfaces. At low pH, CA increased from 106 to 125° as polycarboxylic acid coatings became more hydrophobic. Panels B and C in Figure 3 give an example of pH-triggered transitions observed with PEAA$_{LbL}$-coated surfaces at smooth and microstructured surfaces, and illustrate that oscillations of CA with PEAA$_{LbL}$-coated microstructured substrates were completely reversible when solution pH was cycled in a neutral range between 5 and 7.5. In the case of more hydrophobic PPAA$_{LbL}$ and PBAA$_{LbL}$, the pH was cycled in a more basic range, i.e., between pH 5.5 and 8.3 for PPAA$_{LbL}$, and between pH 7.5 and 9 for PBAA$_{LbL}$.

As shown in Figure 3B, the micropillar structures amplify the changes in CAs. The apparent CAs of patterned (or roughened) surfaces are typically described by the following two models, depending on the wetting state of a droplet on the surfaces. In the case of a Cassie state where a droplet makes a composite interface with the surface (e.g., solid and gas),[11] the apparent CA is typically described by

$$\cos\theta_C = f_{SL}\cos\theta_0 - 1 + f_{SL} \quad (1)$$

where θ_C denotes an apparent CA in the Cassie state, f_{SL} an area fraction of a solid surface wetted by liquid, and θ_0 a CA on a referential, homogeneous and smooth surface. In the case of a Wenzel state where a droplet makes homogeneous contact with a solid surface (i.e., fully wetted with no gas layer entrained),[12] the apparent CA is described by

$$\cos\theta_W = R_f \cos\theta_0 \quad (2)$$

where θ_W denotes an apparent CA on the Wenzel state and R_f a surface roughness factor defined as the ratio of the actual surface area to its flat projection. For the square-array cylindrical pillar pattern as shown in Figure 1b, the f_{SL} and R_f can respectively be estimated

$$f_{SL} = \frac{\pi d^2}{4(d+s)^2} \quad (3)$$

$$R_f = 1 + \frac{\pi d}{(d+s)^2} h \quad (4)$$

where d is the diameter of the pillar tip, s the gap (spacing) between each pillar, and h the pillar height. Thus, the size (d and s) and the height (h) of the micropillar influence the roughness parameters f_{SL} and R_f, and hence the apparent CA θ_C and θ_W. The micropillar-patterned substrate used in Figures 1B, 3, and 5 has pillars that are ~15 μm tall (h) and 5 μm in diameter (d) with 5 μm between pillars in both x and y directions (s_x and s_y). We denote this feature as (d, s_x, s_y) = (5, 5, 5). As supplemental experiments, we fabricated $PEAA_{LbL}$ surface hydrogel on three other kinds of substrates with different interpillar spacing (s), including 10, 20, and 50 μm, but with the fixed tip diameter (d = 5 μm) and height (h = ~15 μm). They are denoted as (d, s_x, s_y) = (5, 10, 10), (5, 20, 20), and (5, 50, 50), respectively. We also measured the CAs as a function of pH on these samples (see Figure S3 in the Supporting Information). The results show that although the interpillar spacing (s) increased, the apparent CAs at low pH decreased significantly, suggesting that the wetting state follows the Wenzel model. The wettability transition pH remained the same and the surface was superhydrophilic at high pHs.

In addition to microscale roughness, surface wetting properties can further be affected by hydrogel swelling and nanoscale roughness of the coatings themselves. To explore this, we have studied the swelling ratio and the surface roughness of the $PMAA_{LbL}$ and $PaAA_{LbL}$ hydrogels at unpatterned substrates using in situ ellipsometry (Figure 4A) and atomic force microscopy (AFM, Figure 4B). At low pH values, $PaAA_{LbL}$ hydrophobic hydrogels uptake a small amount of water (30–45%), whereas $PMAA_{LbL}$ film swelled to as much as twice its dry thickness (Figure 4A). This is a consequence of the different solubility state of PEAA, PPAA and PBAA chains (insoluble and collapsed) from that of PMAA chains (soluble) at acidic pH. At high pH values, the swelling ratio increased for all types of hydrogels, but more hydrophobic $PaAA_{LbL}$ remained much less swollen than $PMAA_{LbL}$ (Figure 4A). At the half-height of CA transitions occurring at $PaAA_{LbL}$-coated micropillar-patterned surfaces at pH 6.2, 7.0, and 8.4 for $PEAA_{LbL}$, $PPAA_{LbL}$ and $PBAA_{LbL}$ films, respectively, the swelling ratio of the coatings was ~2. In the case of the $PMAA_{LbL}$ coating, the swelling ratio remained greater than 2 for the entire pH range. As a result of the larger swelling, stronger swelling-induced interfacial stress and film wrinkling, $PMAA_{LbL}$ hydrogels had higher nanoscale roughness as compared to more hydrophobic $PEAA_{LbL}$, $PPAA_{LbL}$, and $PBAA_{LbL}$ films (Figure 4B and Figure S4 in the Supporting Information).

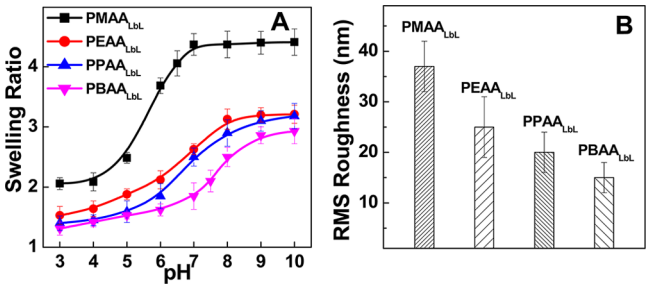

Figure 4. (A) pH dependence of swelling ratios of $PaAA_{LbL}$ films deposited on smooth, unpatterned Si wafers. (B) Root mean square (RMS) roughness of $PaAA_{LbL}$ films exposed to pH 8 buffer obtained by in situ AFM. Representative in situ AFM images are shown in Figure S4 in the Supporting Information.

According to the classical Cassie–Baxter and Wenzel wetting theories (eqs 1 and 2),[11,12] the surface roughness amplifies the apparent CAs so that hydrophobic surfaces become more hydrophobic (superhydrophobic), whereas hydrophilic surfaces become more hydrophilic (superhydrophilic). The Wenzel theory is typically applied in the case when a droplet makes homogeneous contact with roughened solid surface resulting in significant contact line pinning and high CAH, whereas the Cassie–Baxter theory is employed when a droplet makes only partial contact to a roughened surface with the entrapment of air resulting in less contact line pinning and lower CAH. To clarify the exact wettability state of the hydrophobic $PaAA_{LbL}$-coated micropillar-patterned surfaces, we also examined the CAH (Figure 5A), and imaged the behavior of a water droplet on the surface at various pH values using cryo-SEM (Figure 5B-E). At pH < 6, $PEAA_{LbL}$-coated micropillar-structured surfaces demonstrated a CAH of >120°, with a receding CA close to 0°. In this pH range, the droplet is sticky so that it did not slide down or fall off even when the substrates were turned vertically or upside down (see optical images in Figure 5A). Similarly large hysteresis and droplet pinning was observed with $PPAA_{LbL}$ and $PBAA_{LbL}$ hydrogels (data not shown). Such stickiness with high CAH is typical for a droplet in a Wenzel state, resulting from the enhanced contact line pinning by the surface structures. Although a similar phenomenon of strong pinning of water droplets has been reported earlier for different substrates,[45,46] our experiments demonstrate strong, pH-switchable pinning of a droplet on LbL films. Cryo-SEM images (Figure 5B, C) further show that the droplet remains in a complete Wenzel state, with no obvious air bubbles trapped on the micropillared space. This further supports that the sticky behavior of the water droplets at low pH values is because of the enhanced contact line pinning of a droplet boundary by the micropillar structures. Note that although water volume might slightly expand after freezing, we found no difference between the apparent CA of a frozen droplet and that of the initial liquid water droplet. This suggests that the effect of volume change on the wetting state is negligible, if any.

According to the classical Wenzel equation (eq 2), the apparent CA in the Wenzel state should be amplified when the referential CA on a planar surface is greater than 90°. The conventional Wenzel theory uses the apparent CA value of 90° as the hydrophilic-to-hydrophobic transition on smooth surfaces, and also uses the same value to predict the effect of roughness on surface wetting. However, more recent studies in

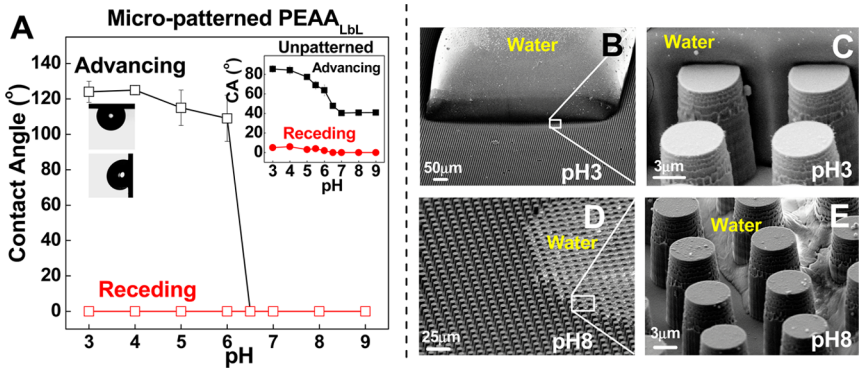

Figure 5. (A) Advancing and receding CAs of PEAA$_{LbL}$ on a micropatterned substrate with a square array of cylindrical pillar structures of ~15 μm tall, 5 μm in diameter, and 5 μm in interpillar spacing. Optical images show water droplets sticking to the substrate at pH 3, suggesting strong pinning. Inset in the upper right corner represents advancing and receding CAs of water droplets on unpatterened substrate. (B–E) Cryo-SEM images of a water droplet on a PEAA$_{LbL}$-coated micropillar-patterned substrate at (B, C) pH 3 and (D, E) pH 8.

biomaterials and polymer science suggest that this value should be reconsidered, possibly to a more experimentally agreeable value of ~65° for a broad set of soft materials.[47] Jiang et al. proposed a modified equation of a Wenzel model, based on the wettability measurements on scraped polymeric surfaces.[48,49] Our experimental data (Figures 2 and Figure 3) show that such amplified transitions with hydrophobic PaAA$_{LbL}$ coatings occur when the apparent CA on an unpatterned surface is ~62–65°, in good agreement with previous reports.[47,48] However, different from these prior studies, we have explored highly swellable coatings (as shown in Figure 4), in which polymer chains might actively adsorb at the water–air interface, changing surface tension and events occurring at the triple phase (solid–gas–liquid) line.[50]

Finally, we have explored the use of PaAA$_{LbL}$ films to detect the presence of positively charged molecules in solution. When 200 μL of antibiotic solutions at concentrations $\geq 2 \times 10^{-3}$ mg/mL (gentamicin in 0.05 M phosphate buffer at pH 6.5) were brought into contact with the PEAA$_{LbL}$ film for 30 min, an increase in CA occurred due to gentamicin binding and neutralization of electrostatic charge within the film, resulting in hydrophobization of the entire hydrogel matrix. Therefore, after gentamicin absorption, static CA increased from ~46 to ~72° on an unpatterned substrate (ellipsometric measurements indicated a 4-nm increase in film dry thickness), and a much stronger change in CA from 0 to ~105° on a micropillar-patterned substrate (Figure 6). Similar changes in CA were

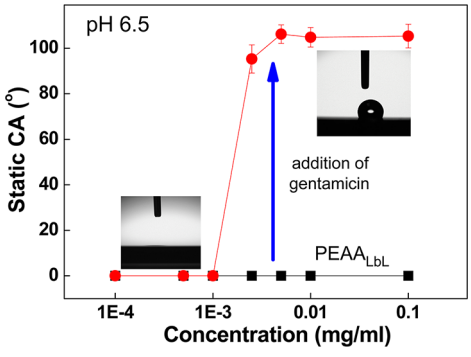

Figure 6. CA changes with PEAA$_{LbL}$-coated micropillar-patterned substrate after exposure to 200 μL of gentamicin solutions at increasing concentration in 0.05 M phosphate buffer at pH 6.5. Arrow indicates an increase in CA resulting from gentamicin binding.

observed with PPAA$_{LbL}$ and PBAA$_{LbL}$ films, when solution pH was adjusted to the pH range of the wetting transition (7.0 and 8.4, respectively). We suggest that the CA measurements with LbL-coated microstructured substrates can be used to detect a wide range of positively charged chemical and biological molecules in aqueous solutions.

CONCLUSIONS

We have demonstrated that deposition of pH-responsive, single-component, LbL-based hydrogels on microstructured substrates presents an efficient way to modify and control surface wetting behavior via changes in pH values. The large-amplitude, highly reversible changes in surface wettability (~120° change in CA) occurred as a result of phase transition of cross-linked polymer chains, and are unlikely to be achieved with conventional LbL films, in which polymer chains are bound together via multisite intermolecular noncovalent interactions. Importantly, with PEAA$_{LbL}$ coatings, the wettability transition occurred in a physiologically relevant pH range. This feature opens ways to use such coatings to control adhesion of cells and biological molecules at surfaces. The suggested approach of constructing LbL coatings can be extended to a large number of polymers which undergo collapse-solubility transitions in response to variations of solution pH or temperature. We have demonstrated that the use of polymers of varied hydrophobicity enables control of the transition on the pH scale. Moreover, pH-triggered changes in wettability might be useful for controlling flow within microfluidic devices, whereas controllable switching between droplet pinning and surface wetting states, as well as analyte-induced changes in surface wettability can find applications in chemical and biological lab-on-a-chip technologies.

ASSOCIATED CONTENT

Supporting Information

FTIR spectra, thickness change, roughness effect, and AFM images. This material is available free of charge via the Internet at http://pubs.acs.org.

AUTHOR INFORMATION

Corresponding Authors

*E-mail: ssukhish@stevens.edu. Phone: 201-216-5544.
*E-mail: cchoi@stevens.edu. Phone: 201-216-5579.

Notes

The authors declare no competing financial interest.

■ ACKNOWLEDGMENTS

We thank Stevens Institute of Technology for their financial support through the Technogenesis® fellowship program (Y.L.). This work was partially supported by the National Science Foundation under Award DMR-0906474 (S.A.S.) and the U.S. Office of Naval Research under Young Investigator Program (Award N00014-10-1-0751) and Defense University Research Instrumentation Program (Award N00014-11-1-0841) (C.-H.C.).

■ REFERENCES

(1) Chen, F.; Zhang, D.; Yang, Q.; Yong, J.; Du, G.; Si, J.; Yun, F.; Hou, X. *ACS Appl. Mater. Interfaces* **2013**, *5*, 6777−6792.
(2) Erbil, H. Y.; Demirel, A. L.; Avcı, Y.; Mert, O. *Science* **2003**, *299*, 1377−1380.
(3) Choi, C.-H.; Kim, C.-J. *Phys. Rev. Lett.* **2006**, *96*, 066001.
(4) Xu, W.; Choi, C.-H. *Phys. Rev. Lett.* **2012**, *109*, 024504.
(5) Liu, Y.; Choi, C.-H. *Colloid Polym. Sci.* **2013**, *291*, 437−445.
(6) Onda, T.; Shibuichi, S.; Satoh, N.; Tsujii, K. *Langmuir* **1996**, *12*, 2125−2127.
(7) Feng, L.; Li, S.; Li, Y.; Li, H.; Zhang, L.; Zhai, J.; Song, Y.; Liu, B.; Jiang, L.; Zhu, D. *Adv. Mater.* **2002**, *14*, 1857−1860.
(8) Tuteja, A.; Choi, W.; Ma, M.; Mabry, J. M.; Mazzella, S. A.; Rutledge, G. C.; McKinley, G. H.; Cohen, R. E. *Science* **2007**, *318*, 1618−1622.
(9) Genzer, J.; Efimenko, K. *Biofouling* **2006**, *22*, 339−360.
(10) Ju, J.; Bai, H.; Zheng, Y.; Zhao, T.; Fang, R.; Jiang, L. *Nat. Commun.* **2012**, *3*, 1247.
(11) Cassie, A. B. D.; Baxter, S. *Trans. Faraday Soc.* **1944**, *40*, 546−551.
(12) Wenzel, R. N. *Ind. Eng. Chem.* **1936**, *28*, 988−994.
(13) Liu, X.; Liang, Y.; Zhou, F.; Liu, W. *Soft Matter* **2012**, *8*, 2070−2086.
(14) Choi, W.; Tuteja, A.; Chhatre, S.; Mabry, J. M.; Cohen, R. E.; McKinley, G. H. *Adv. Mater.* **2009**, *21*, 2190−2195.
(15) Olivero, G.; Maiolo, D.; Leali, D.; Federici, S.; Depero, L. E.; Presta, M.; Mitola, S.; Bergese, P. *Biosens. Bioelectron.* **2010**, *26*, 1571−1575.
(16) Feng, X.; Feng, L.; Jin, M.; Zhai, J.; Jiang, L.; Zhu, D. *J. Am. Chem. Soc.* **2003**, *126*, 62−63.
(17) Lai, Y.; Pan, F.; Xu, C.; Fuchs, H.; Chi, L. *Adv. Mater.* **2013**, *25*, 1682−1686.
(18) Pernites, R. B.; Ponnapati, R. R.; Advincula, R. C. *Adv. Mater.* **2011**, *23*, 3207−3213.
(19) Grigoryev, A.; Tokarev, I.; Kornev, K. G.; Luzinov, I.; Minko, S. *J. Am. Chem. Soc.* **2012**, *134*, 12916−12919.
(20) Lim, H. S.; Han, J. T.; Kwak, D.; Jin, M.; Cho, K. *J. Am. Chem. Soc.* **2006**, *128*, 14458−14459.
(21) Yu, X.; Wang, Z.; Jiang, Y.; Shi, F.; Zhang, X. *Adv. Mater.* **2005**, *17*, 1289−1293.
(22) Xia, F.; Jiang, L. *Adv. Mater.* **2008**, *20*, 2842.
(23) Sun, T.; Wang, G.; Feng, L.; Liu, B.; Ma, Y.; Jiang, L.; Zhu, D. *Angew. Chem., Int. Ed.* **2004**, *43*, 357−360.
(24) Zhang, Q.; Xia, F.; Sun, T.; Song, W.; Zhao, T.; Liu, M.; Jiang, L. *Chem. Commun.* **2008**, *10*, 1199−1201.
(25) Xia, F.; Feng, L.; Wang, S.; Sun, T.; Song, W.; Jiang, W.; Jiang, L. *Adv. Mater.* **2006**, *18*, 432−436.
(26) Decher, G.; Hong, J. D.; Schmitt, J. *Thin Solid Films* **1992**, *210*, 831−835.
(27) Decher, G. *Science* **1997**, *277*, 1232−1237.
(28) Zhai, L.; Cebeci, F. Ç.; Cohen, R. E.; Rubner, M. F. *Nano Lett.* **2004**, *4*, 1349−1353.
(29) Li, Y.; Li, L.; Sun, J. *Angew. Chem., Int. Ed.* **2010**, *49*, 6129−6133.
(30) Tasuku, O.; Bin, D.; Yuji, S.; Seimei, S. *Nanotechnology* **2007**, *18*, 165607.
(31) Amigoni, S.; Taffin de Givenchy, E.; Dufay, M.; Guittard, F. d. r. *Langmuir* **2009**, *25*, 11073−11077.
(32) Liao, K.-S.; Wan, A.; Batteas, J. D.; Bergbreiter, D. E. *Langmuir* **2008**, *24*, 4245−4253.
(33) Jisr, R. M.; Rmaile, H. H.; Schlenoff, J. B. *Angew. Chem., Int. Ed.* **2005**, *44*, 782−785.
(34) Yoo, D.; Shiratori, S. S.; Rubner, M. F. *Macromolecules* **1998**, *31*, 4309−4318.
(35) Hemmerlé, J.; Roucoules, V.; Fleith, G.; Nardin, M.; Ball, V.; Lavalle, P.; Marie, P.; Voegel, J. C.; Schaaf, P. *Langmuir* **2005**, *21*, 10328−10331.
(36) Kwak, D.; Han, J. T.; Lee, J. H.; Lim, H. S.; Lee, D. H.; Cho, K. *Surf. Sci.* **2008**, *602*, 3100−3105.
(37) Wang, L.; Peng, B.; Su, Z. *Langmuir* **2010**, *26*, 12203−12208.
(38) Yang, J.; Zhang, Z.; Men, X.; Xu, X.; Zhu, X.; Zhou, X. *Langmuir* **2011**, *27*, 7357−7360.
(39) Kharlampieva, E.; Sukhishvili, S. A. *Polymer Rev.* **2006**, *46*, 377−395.
(40) Yang, S. Y.; Rubner, M. F. *J. Am. Chem. Soc.* **2002**, *124*, 2100−2101.
(41) Pavlukhina, S.; Lu, Y.; Patimetha, A.; Libera, M.; Sukhishvili, S. *Biomacromolecules* **2010**, *11*, 3448−3456.
(42) Lu, Y.; Zhuk, A.; Xu, L.; Liang, X.; Kharlampieva, E.; Sukhishvili, S. A. *Soft Matter* **2013**, *9*, 5464−5472.
(43) Ferritto, M. S.; Tirrell, D. A. *Macrom. Synth.* **1992**, *11*, 59−62.
(44) Peljhan, S.; Žagar, E.; Cerkovnik, J.; Kogej, K. *J. Phys. Chem. B* **2009**, *113*, 2300−2309.
(45) Winkleman, A.; Gotesman, G.; Yoffe, A.; Naaman, R. *Nano Lett.* **2008**, *8*, 1241−1245.
(46) Jin, M.; Feng, X.; Feng, L.; Sun, T.; Zhai, J.; Li, T.; Jiang, L. *Adv. Mater.* **2005**, *17*, 1977−1981.
(47) Vogler, E. A. *Adv. Colloid Interface Sci.* **1998**, *74*, 69−117.
(48) Guo, C.; Wang, S.; Liu, H.; Feng, L.; Song, Y.; Jiang, L. *J. Adhes. Sci. Technol.* **2008**, *22*, 395−402.
(49) Tian, Y.; Jiang, L. *Nat. Mater.* **2013**, *12*, 291−292.
(50) Cohen Stuart, M. A.; de Vos, W. M.; Leermakers, F. A. M. *Langmuir* **2006**, *22*, 1722−1728.